RESEARCH ARTICLE

Optimized Design of LCL Filters for Single-Phase Grid-Connected Inverter Systems using Advanced Optimization Techniques

Imad Hussain[1], **Yigang He**[1,*], **Atta Ullah Khan**[1], **Yaqoob Ali**[2] **and Idrees Khan**[3]

[1] The State Key Laboratory of Power Grid Environmental Protection, School of Electrical Engineering and Automation, Wuhan University, Wuhan 430072, China
[2] Department of Electrical Engineering, Shanghai Jiao Tong University, Shanghai 200240, China
[3] School of Automation and Electrical Engineering, Zhejiang University of Science and Technology, Hangzhou 310023, China

Abstract

AI-driven metaheuristic optimization algorithms have demonstrated strong potential in solving complex, high-dimensional engineering design problems. This paper applies and systematically compares three representative swarm-intelligence and evolutionary computation methods— particle swarm optimization (PSO), whale optimization algorithm (WOA), and grey wolf optimizer (GWO)—to the parameter design of LCL filters in single-phase grid-tied inverter systems, a class of problems characterized by nonlinear constraints and competing performance objectives. A structured optimization framework is developed, incorporating an objective function targeting total harmonic distortion (THD) minimization and three engineering constraints governing inductance bounds, damping power loss, and resonance frequency range. Computational and simulation results analyzed under multiple operating conditions—including step-change transients and weak-grid short-circuit faults—demonstrate that PSO achieves superior convergence behavior, lower fitness values, and better robustness compared to WOA and GWO, while ensuring full compliance with IEEE 519 harmonic standards. The findings provide quantitative insights into the comparative computational performance of these algorithms on a constrained continuous optimization problem with direct industrial applicability.

Keywords: swarm intelligence, evolutionary computation, AI-driven optimization, metaheuristic algorithms, constrained parameter optimization, LCL filter design, weak grid.

1 Introduction

LCL filters are widely employed in distributed energy generation systems, including grid-connected inverters (GCIs), owing to their remarkable

Submitted: 02 June 2025
Revised: 13 August 2025
Accepted: 16 October 2025
Published: 05 April 2026

Vol. 2, **No.** 3, 2026.
10.62762/TACS.2025.424683

***Corresponding author:**
Yigang He
Yghe1221@whu.edu.cn

Citation
Hussain, I., He, Y., Khan, A. U., Ali, Y., & Khan, I. (2026). Optimized Design of LCL Filters for Single-Phase Grid-Connected Inverter Systems using Advanced Optimization Techniques. *ICCK Transactions on Advanced Computing and Systems*, 2(3), 158–172.

© 2026 by the Authors. Published by Institute of Central Computation and Knowledge. This is an open access article under the CC BY license (https://creativecommons.org/licenses/by/4.0/).

high-frequency (HF) rejection capabilities, small form factor, and cost-effectiveness [1, 4]. These advantages have been demonstrated across both three-phase [2, 3] and single-phase converter configurations [5, 6]. Designing an accurate and dependable LCL filter is essential for realizing reduced costs, improved filtering performance, and high-quality current.

The traditional approach to LCL filter design relies on trial-and-error methodology. This method first determines the component boundaries based on constraints such as total harmonic distortion (THD), current ripple, and impedance stability considerations [5, 6, 8]. The damping design of the LCL filter further requires careful selection of passive damping elements to limit resonance amplification across a wide range of filter configurations [7]. The filter parameter design also requires establishing safe operating regions for the current controller to ensure stability across both grid-side and inverter-side control modes [6]. Then, a specific configuration of filter components is chosen and implemented in the real-world system. If the necessary grid connection requirements are not met, the LCL filter components and control parameters are iteratively adjusted and validated against multiple constraints—including stability, resonance suppression, and bandwidth margins—until the design goals are achieved [9–12]. Recent research has explored enhancements to this trial-and-error method. For instance, [13] proposed an optimal ratio between switching and resonance frequencies, considering a broad range of design limitations, which effectively narrows the set of possible solutions. Reference [14] further proposes an optimum capacitance selection method based on reactive power compensation, minimizing the total filter inductance while satisfying IEEE-519 harmonic limits. References [15] and [16] also suggest some new and improved constraints. The trial-and-error method, despite its ability to reduce the range of potential filter components values, has notable limitations. Therefore, the filter configurations in each iteration are selected based on the engineer's subjective judgment and past experience, and the ultimate LCL component values may be established after numerous trials. This makes it challenging to predict the performance of the LCL filter design. Furthermore, the resulting component values may not always be the optimal solution, as they merely represent a set of solutions that satisfy the verification conditions [17].

In addition to the traditional trial-and-error approach, there are more advanced methods for designing LCL filter components. One such method is the iterative approach, which involves gradually adjusting the constraints of a defined governing equation, such as the harmonic distortion in the current [17] or the current ripple [18], to find the appropriate filter components that meet all the criteria. However, like the trial-and-error method, the iterative approach has certain limitations. On the other hand, the graphical approach can also be employed for filter component design [20]. This approach involves creating a graphical representation of the relationships between the filter components and key measurements like damping ability, sizes, and budget. The resulting graph provides a visual interaction curve that allows for the selection of the optimal filter components based on the desired performance requirements. Such optimization-oriented design strategies are particularly valuable under variable grid conditions, including weak grids [19].

Additionally, genetic algorithm-based optimization techniques have been explored for LCL filter component design. These approaches use developed optimization techniques with different constraints to model the LCL filter components. The THD [21] and the current ripple rate [22, 23] are incorporated as components of the multi-objective optimization function. The LCL filter components are then optimized using genetic algorithms and particle swarm optimization (PSO), respectively. However, the authors have not established the upper and lower boundaries for the LCL filter components, which could result in a higher cost and a larger LCL filter.

The existing design methodologies for LCL filters confront several substantial obstacles. Firstly, the design progression lacks a comprehensive examination of the damping factor, which remains a crucial determinant in ascertaining the LCL filter's resonance frequency. Secondly, industry standards such as IEEE 519 [24] and IEEE 1547 [25] impose restrictions on the THD of the current, in addition to the harmonic distortion within defined frequency bands, as depicted in Table 1. Ultimately, to minimize the expense of the LCL filter, the design components and damping mechanism must operate effectively under grid disturbances and tolerate fluctuations in the control signal. This is crucial for ensuring cost-effectiveness and reliable operation. However, previous studies have not adequately addressed these aspects [26].

In recent years, AI-driven metaheuristic algorithms

Table 1. IEEE 519 harmonic limits for injected current [24].

Harmonic-order (h)	$(h) < 11.0$	$11.0 \leq (h) < 17.0$	$17.0 \leq (h) < 23$	$23.0 \leq (h) < 35.0$	$35.0 \leq (h)$	THD
Current ratio (%)	4.0	2.0	1.5	0.6	0.3	5.0

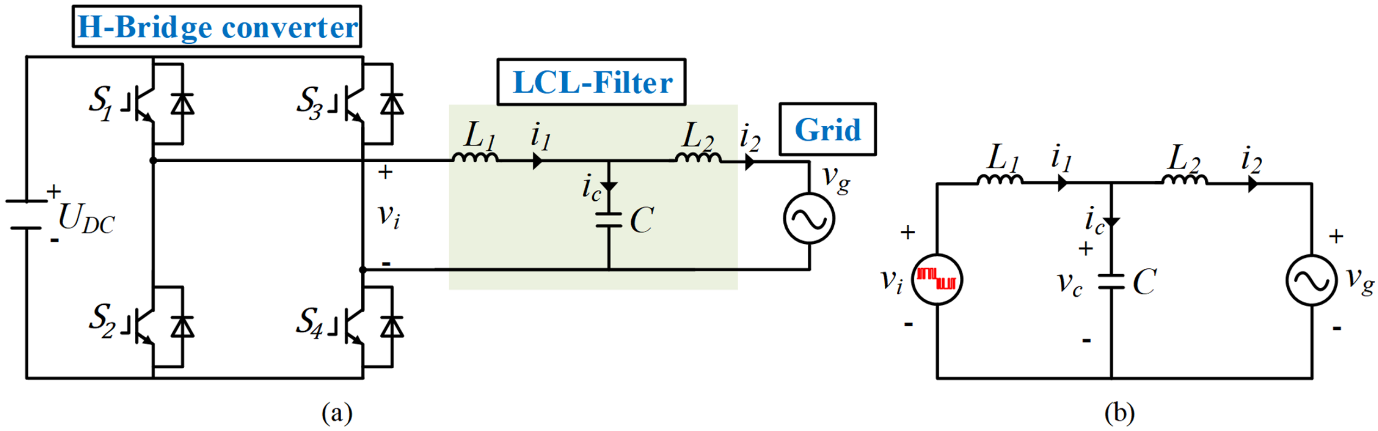

Figure 1. Single-phase GCI with LCL filter: (a) system diagram (b) equivalent diagram.

have emerged as powerful computational tools for resolving complex engineering design problems, including LCL filter parameter optimization for grid-connected inverters [19–22], particularly under variable grid conditions where conventional analytical methods prove insufficient. These algorithms surpass traditional design techniques by exploiting distinctive computational search strategies—including swarm intelligence, evolutionary computation, and bio-inspired behavioral modeling—to efficiently navigate high-dimensional, nonlinearly constrained solution spaces. This paper focuses on three representative algorithms: the grey wolf optimizer (GWO) [29], which models the hierarchical hunting behavior of wolf packs; the particle swarm optimization (PSO) [28], which simulates collective social intelligence in bird flocking; and the whale optimization algorithm (WOA) [27], which replicates the spiral bubble-net feeding strategy of humpback whales. A rigorous computational comparison of these three algorithms is conducted with respect to convergence speed, fitness value, parameter quality, and system robustness under transient and weak-grid conditions, using Simulink/MATLAB as the simulation platform.

The remainder of the work is constructed as follows: Section 2 presents a comprehensive explanation of the modeling and analysis of the LCL-filtered single-phase GCI. The objective functions and constraints governing the design of the LCL and damping components are outlined in Section 3. Section 4 introduces the specified MHTs and presents their mathematical formulations. The selection of the optimum values and the effect of simulated MHTs are shown in Section 5. The simulation results under different grid conditions are given in Section 6. In conclusion, a summary of the key findings is presented in Section 7.

2 Harmonic Current Behavior in Single-Phase GCI with LCL Filter

Figure 1(a) shows a single-phase grid-tied inverter system using an LCL filter. The inverter, powered by a DC source representing a renewable energy source, produces an AC voltage (v_i). This voltage is then filtered by the LCL filter, which consists of an inductor (L_1) on the inverter side, a capacitor (C), and an inductor (L_2) on the grid side. The currents in the system are labeled as follows: i_1 for the inverter side current, i_2 for the grid side current, and i_c for the capacitor current. For simplicity, the grid inductance is combined with the LCL filter's grid-side inductance (L_2), assuming the grid voltage (v_g) is equal to the point of common coupling (PCC) voltage (v_{pcc}).

Simplifying Figure 1(a) results in Figure 1(b), where the transfer function from the inverter voltage $v_i(s)$ to the grid current $i_2(s)$ is provided by [30]:

$$G_{LCL}(s) = G_{i2}(s) = \frac{I_2(s)}{V_i(s)} = \frac{1}{L_1 L_2 C} \cdot \frac{1}{s^2 + \omega_{\text{res}}^2} \quad (1)$$

where ω_{res} denotes the angular resonance frequency and is outlined as:

$$\omega_{\text{res}} = \sqrt{\frac{L_1 + L_2}{L_1 L_2 C}} \quad \text{or} \quad f_{\text{res}} = \frac{1}{2\pi}\sqrt{\frac{L_1 + L_2}{L_1 L_2 C}} \quad (2)$$

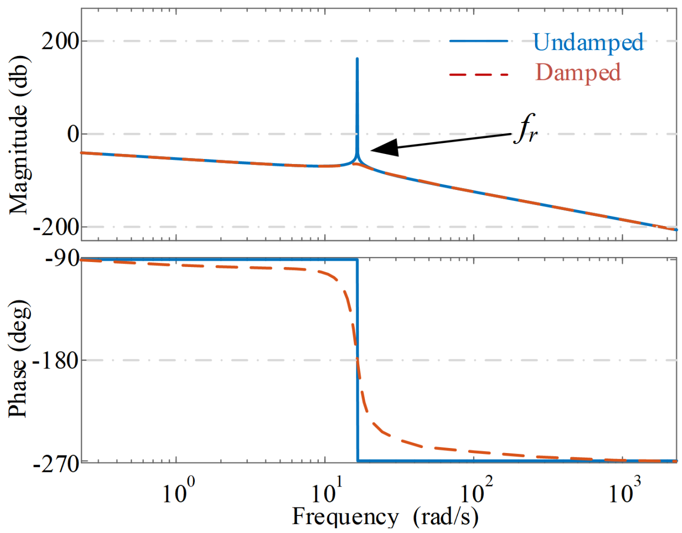

Figure 2. Frequency response of $G_{LCL}(s)$ and $G_{LCL_d}(s)$.

In Figure 2, the solid line depicts the frequency response of $G_{LCL}(s)$ according to (1). A high resonance peak is observed at the resonance frequency f_{res}, which results in a sharp phase step down of $-180°$. From a control standpoint, this $-180°$ crossover is negative, and it will result in two closed-loop right-half-plane poles, which cause system instability [31]. In order to prevent the negative $-180°$ crossover and maintain system stability, the resonance peak must be reduced below 0 dB. To dampen the resonance peak, an s term must be added to the resonant terms in the denominator of (1), which gives [32]:

$$G_{LCL\_d}(s) = \frac{I_2(s)}{V_i(s)} = \frac{1}{L_1 L_2 C} \cdot \frac{1}{s^2 + 2\zeta s \omega_{\text{res}} + \omega_{\text{res}}^2} \tag{3}$$

where ζ is the damping ratio. The dashed line in Figure 2 represents the Bode diagram of $G_{LCL\_d}(s)$ in accordance with equation (3). It is clear that adding the damping term successfully suppresses the resonance peak of the LCL filter. The passive damping method is a straightforward way to dampen the resonance by inserting a resistor into the filter system. There are six standard passive-damping options based on the resistor position [31].

This work selects the non-edge damping of capacitor series resistance as depicted in Figure 3(a), where v_{i1} and v_{ih} are the fundamental and harmonic components of the input voltage of the LCL filter, while R_d is the resistor used to attenuate the resonance frequency. The main goal of LCL-filter design is typically the attenuation of HFs. At the initial stages of the LCL-filter design process, the fundamental components of the input voltage of the LCL filter and the grid voltage are ignored as shown in Figure 3(b). The transfer functions from the harmonic components of the input voltage to i_1 and i_2 are given as follows:

$$\begin{aligned} G_{i_{1h}/v_{ih}}(s) &= \frac{I_{1,h}(s)}{V_{i,h}(s)} \\ &= \frac{L_2 C s^2 + R_d C s + 1}{L_1 L_2 C s^3 + (L_1 + L_2) R_d C s^2 + (L_1 + L_2) s} \end{aligned} \tag{4}$$

$$\begin{aligned} G_{i_{2h}/v_{ih}}(s) &= \frac{I_{2,h}(s)}{V_{i,h}(s)} \\ &= \frac{R_d C s + 1}{L_1 L_2 C s^3 + (L_1 + L_2) R_d C s^2 + (L_1 + L_2) s} \end{aligned} \tag{5}$$

$$\delta_{i_{2h}/i_{1h}}(s) = \frac{I_{2,h}(s)}{I_{1,h}(s)} = \frac{R_d C s + 1}{L_2 C s^2 + R_d C s + 1} \tag{6}$$

The transfer function in equation (6) reflects the attenuation capability of the LCL filter for a defined harmonic frequency, showing the relationship between the currents in the inverter side and the grid side of the LCL filter. This transfer function will be used to build the subsequent optimization problem.

3 Parameter Optimization of LCL-filter

3.1 Optimization Variables and Constraint Conditions

The inverter-side inductor L_1, capacitor C, grid-side inductor L_2, and damping resistor R_d are the four variables chosen to be optimized in this work. The effectiveness of the LCL-filter component optimization might be considerably enhanced if an intelligent method is used to choose the appropriate ranges to consider for the components to optimize.

Regarding the total inductance L_T, a high value improves the LCL filtering performance since it decreases the current ripples. Nevertheless, the total inductance should not be too high since it would lower the power factor and progressively raise the voltage drop across the inductor, both of which would reduce the power transmission capability of the inverter. As a result, the LCL-filter total inductance L_T has an upper limit:

$$L_{\max} = \frac{\alpha U_{gm}^2}{\omega_L P_N} \tag{7}$$

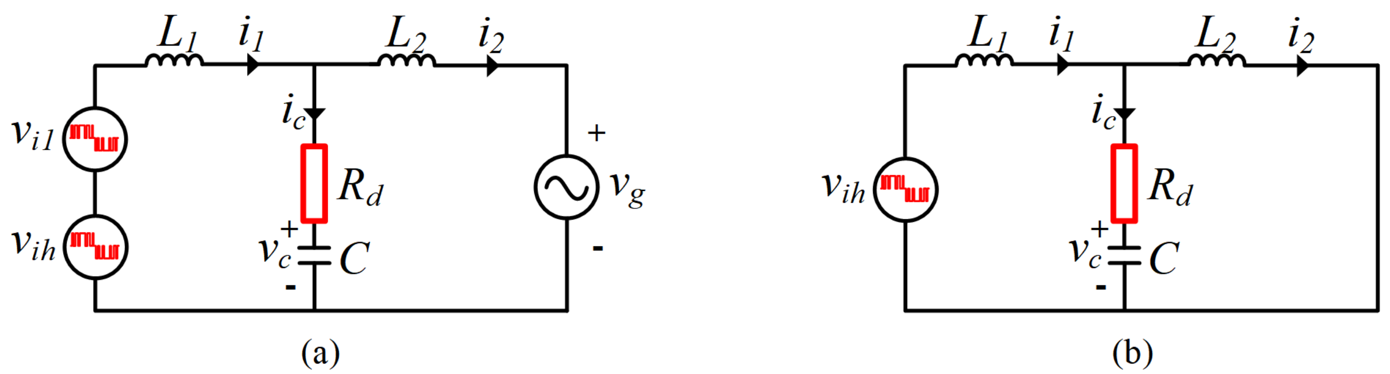

Figure 3. Equivalent Circuit of LCL-filtered GCI including passive damping.

where $\omega_L = 2\pi f_L$ is the angular fundamental frequency of the grid, U_{gm} is the peak value of the grid voltage, P_N is the rated active power, and α is the maximum allowable ratio of the inductive voltage drop to the grid voltage (typically $\alpha = 0.1$, i.e., 10%). Therefore, the total-inductance range to consider for the optimization is $(0, L_{\max})$.

The possible ranges of the inductances in the inverter side L_1 and the grid side L_2 should also be established. The inductor ripple current has to be kept to a limit because it increases the switching and conduction losses in the inverter switches. Furthermore, because the capacitance is low at HFs and the filter capacitor provides the discharge path for the HF harmonics, the capacitor C and the grid-side inductor L_2 have a low parallel impedance. The parallel impedance between C and L_2 is negligible due to the low inductance of L_2 in the low-frequency (LF) region. Therefore, the amount of the L_1 ripple current is mostly determined by the size of the inverter-side inductor. Generally, the L_1 ripple-current amplitude $I_{L,1,\text{peak}}$ must be less than 20% of the current peak value I_{gm}. As a result, the lower limit of L_1 is given as follows:

$$L_{1,\min} \geq \frac{U_{DC}}{2\Delta I_{L,1,\text{peak}} f_{sw}} \tag{8}$$

where f_{sw} is the switching frequency. As a result, the possible boundaries of L_1 and L_2 are found to be $L_1 \in (L_{1,\min}, L_{\max})$ and $L_2 \in (0, L_{\max})$.

Lastly, the possible range for the capacitor C is also defined. Increasing filter capacitance increases the capability of the LCL filter to attenuate HF signals. However, a high capacity will cause the reactive power to rise, which will result in a low power factor for the overall system. Hence, for the single-phase system considered here, the reactive power generated by the filter capacitance must normally not be greater than 5% of the rated active power, i.e.,

$$\omega_L C v_{g,\text{rms}}^2 < 5\% \cdot P_N \tag{9}$$

where v_c is the filter capacitor voltage. The root mean square (rms) value of the grid voltage $v_{g,\text{rms}}$ is utilized to set the upper bound of the filter capacitor because the voltage drop across L_2 is negligible and may be disregarded. The capacitance maximum value is then determined as:

$$C_{\max} < \frac{P_N}{\omega_L v_{g,\text{rms}}^2} \tag{10}$$

Therefore, the viable limit for the capacitor is $C \in (0, C_{\max})$.

3.2 Objective Function

Optimizing the LCL filter components requires the following considerations:

- When optimizing the LCL filter components, it's important to consider the impact of the current controller. By carefully tuning the current controller, we can significantly reduce LF harmonic contents in the injected current. This is because the controller primarily operates on LF signals due to its limited bandwidth.
- Meeting the THD limit for current is a significant challenge. As Table 1 illustrates, if THD reduction isn't a primary design goal for the LCL filter, the resulting current distortion may not comply with grid integration standards like IEEE 519.

Given these facts, this paper focuses on the importance of the THD of the current in the LCL-filter component design. To meet the criterion for the THD limit of the current, equation (6) is modified to achieve minimum current attenuation proportional coefficient in the complex frequency domain as:

$$\min|\delta(\omega_n)| = \frac{R_d C j\omega_n + 1}{-L_2 C\omega_n^2 + R_d C j\omega_n + 1} \tag{11}$$

$$= \frac{(h+1)R_d C j\omega_n + h + 1}{h + 1 - L_2 C\omega_n^2 + (h+1)R_d C j\omega_n} \tag{12}$$

where h represents the harmonic order and ω_n denotes the nth harmonic angular frequency. The value of equation (11) should be near zero for effective harmonic minimization. A value that is close to zero indicates that the magnitude of each current harmonic $h_1, h_2, h_3, \ldots, h_n$ in $i_{2,h}$ is reduced to nearly zero.

3.3 Constraint

3.3.1 *Constraint 1*

To ensure that the overall inductance is below $L_{\max}$, the algorithm should follow the following equation for the two-inductance value:

$$L_1 + L_2 \leq L_{\max} \tag{13}$$

3.3.2 *Constraint 2*

The key concern for passive damping is the amount of power loss due to the damping resistor [31]. For the single-phase system considered in this work, the power dissipated in the damping resistor R_d connected in series with the filter capacitor is given by the following equation, which is used to ensure that the loss remains below the prescribed limit $P_{L,\min}$ and to bound the admissible range of R_d:

$$P_{L,\min} = R_d \frac{v_g^2}{R_d^2 + \frac{1}{\omega_L^2 C^2}} \tag{14}$$

where ω_L is the angular fundamental frequency of the grid.

3.3.3 *Constraint 3*

In general, a low value of the LCL-filter resonance frequency f_r increases the LF current harmonics in the current, while a high value causes the current harmonics to increase near the switching frequency f_{sw}. Hence, the f_r should be in the medium-frequency range, above the controller bandwidth but below the switching frequency. Thus, f_r should be calculated to fall within the following range:

$$10f_L < f_r < 0.5f_{sw} \tag{15}$$

4 Metaheuristic Optimization Techniques

This work utilizes three MHTs –WOA, PSO, and GWO – to optimize the components of LCL filter and damping resistor. A detailed description of each algorithm is provided below.

4.1 Whale Optimization Algorithm

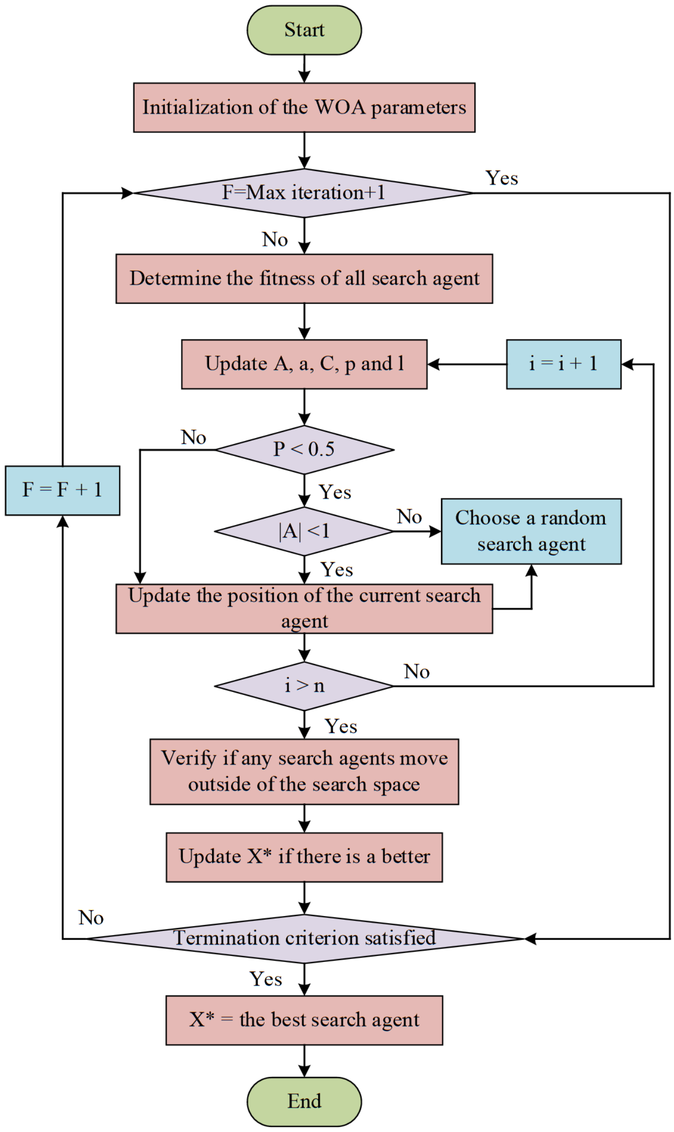

Figure 4. Flowchart of WOA [27].

The WOA is an advanced MHA inspired by the unique hunting strategy of humpback whales, known as the spiral bubble net feeding method [27]. In this method, whales create distinctive spiral-shaped bubbles to encircle and trap their prey. The flow chart for WOA is illustrated in Figure 4. The agents in the algorithm randomly follow the prey (optimal solutions) based on their relative positions. This dynamic following behavior is mathematically represented through two main mechanisms: the spiral revised location and the decreasing encircling method. These mechanisms are described in [27] and are formulated as follows:

$$X(t+1) = \begin{cases} X^*(t) - \vec{A}\vec{D} & \text{if } p < 0.5 \\ D' e^{bl} \cos(2\pi l) + X^*(t) & \text{if } p \geq 0.5 \end{cases} \quad (16)$$

$$\vec{D} = |\vec{B}X_i^*(t) - \vec{X}(t)| \quad (17)$$

$$\vec{A} = r\vec{B} - \vec{r}_o \quad (18)$$

where $X(t+1)$ is the position of the whale at the next time step, X^* is the current position of the best solution found so far, p is a random number in the range $[0, 1]$, $\vec{D}$ and D' represent the distance between the whale and the prey, $\vec{A}$ and $\vec{B}$ are coefficient vectors.

4.2 Grey Wolf Optimization

The GWO is designed to mimic the common hierarchy and collaborative hunting mechanism of grey wolves [29]. This MHA uses mathematical models to simulate the way wolves encircle and hunt their prey. The flow chart for GWO is shown in Figure 5. The key equations of the GWO are structured to represent the movements of different wolves in the pack towards the prey, based on their social ranking:

Equation (19) calculates the distance D between a wolf's current position $X(t)$ and the prey's position X_p adjusted by coefficient vectors A and B.

$$D = |BX_p - AX(t)|_\omega \quad (19)$$

Equation (20) updates the wolf's position:

$$X(t+1) = X_p(t) - AD_\omega \quad (20)$$

The positions of alpha (X_α), beta (X_β) and delta (X_δ) wolves are updated using their respective equations to simulate their influence on the hunt:

Equation (21) for the alpha wolf $(\overline{X}_1)$:

$$\vec{X}_1 = \vec{X}_\alpha - A_1^*(\vec{D}_\alpha)_\omega \quad (21)$$

Equation (22) for the beta wolf $(\overline{X}_2)$:

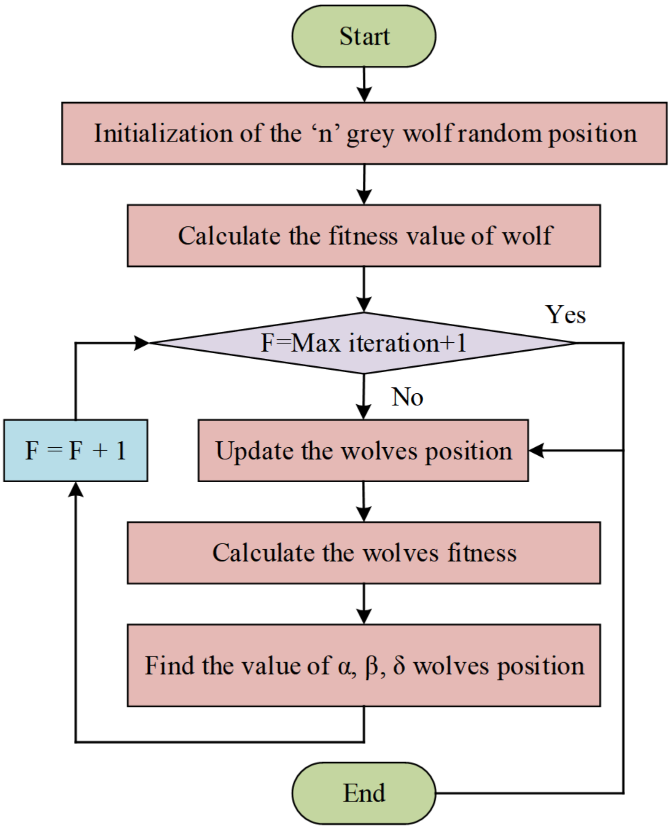

Figure 5. Flowchart of GWO [29].

$$\vec{X}_2 = \vec{X}_\beta - A_2^*(\vec{D}_\beta)_\omega \quad (22)$$

Equation (23) for the delta wolf $(\overline{X}_3)$:

$$\vec{X}_3 = \vec{X}_\delta - A_3^*(\vec{D}_\delta)_\omega \quad (23)$$

Finally, the position of any wolf within the pack is updated by averaging the positions influenced by the alpha, beta, and delta wolves, as given in equation (24):

$$\vec{X}(t+1) = \frac{X_1 + X_2 + X_3}{3} \quad (24)$$

where $X(t+1)$ represents the wolf's location at the subsequent time step, D represents the distance between the wolf's current location and the prey, influenced by the dynamic coefficients A and B.

4.3 Particle Swarm Optimization

The PSO algorithm is a population-based optimization tool that simulates the social behavior observed in flocks of birds or schools of fish [28]. In PSO, each individual within the swarm represents a particle that adjusts its position in the search space according to

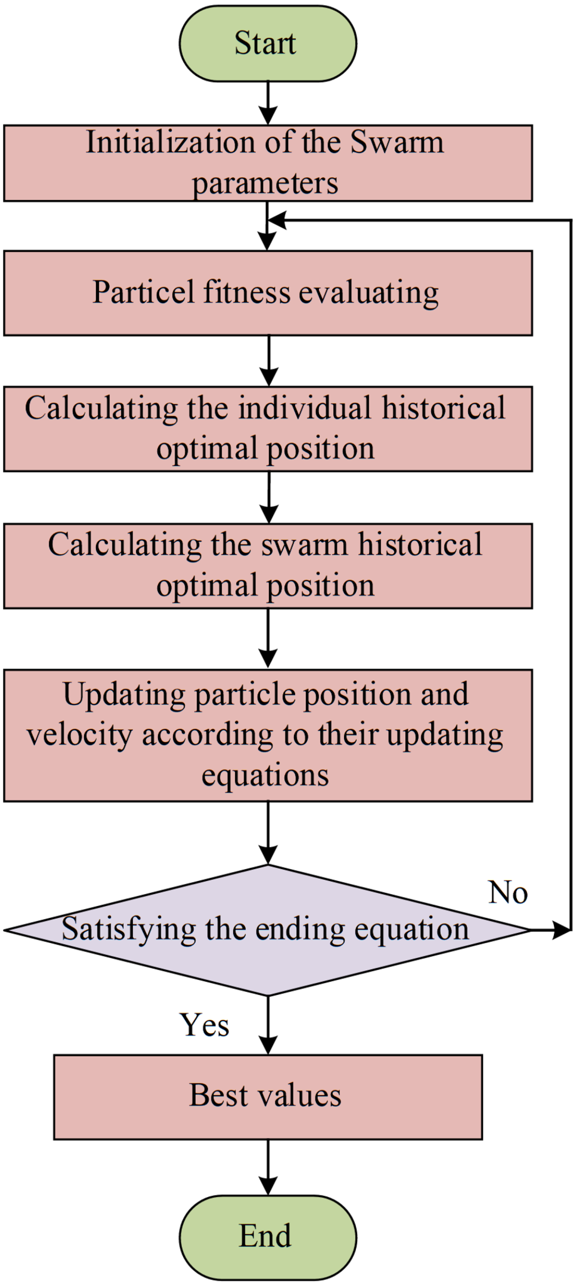

Figure 6. Flowchart of PSO [28].

its own experience and that of its neighbors. The flow chart for PSO is shown in Figure 6 [28]. Each particle aims to find the optimal solution by adjusting its trajectory towards two key positions:

P_i : The best position visited by the particle itself so far, determined by:

$$P_i = \arg\min\left[f(X_i)\right] \tag{25}$$

where $f(X_i)$ is the value of the objective function at the particle's position X_i.

G_i : The best global position discovered by the entire swarm at iteration i, defined by:

$$G_i = \arg\min\left[f(X_i)\right] \tag{26}$$

The velocity of each particle is updated as follows:

$$V_{i+1} = \omega V_i + c_1 r_1 (P_i - X_i) + c_2 r_2 (G_i - X_i) \tag{27}$$

where ω is the inertia weight which controls the particle's previous velocity, contributing to the momentum of the particles. The constants c_1 and c_2 are acceleration coefficients that control the relative influence of the personal best and global best, respectively. r_1 and r_2 are random variables uniformly distributed within $[0, 1]$, introducing stochastic elements to the velocity. The position of each particle is updated as follows:

$$X_{i+1} = X_i + V_{i+1} \tag{28}$$

Equation (28) adjusts the particle's position (X_{i+1}) based on its updated velocity (V_{i+1}), effectively moving the particle through the search space. Equations (27) and (28) allow the PSO algorithm to navigate efficiently through the search space toward the optimal solution, adapting based on individual and global experiences of the particles.

5 LCL Components and Damping Resistance Optimization

This study aims to develop a process that determines the optimal values for the LCL components and damping resistor, resulting in a GCI with high-quality grid current. Based on the GCI parameters in Table 2 and equations (7), (8), and (10), with $\alpha = 0.1$, the maximum allowable total inductance is $L_{\max} \approx 6.16\,\text{mH}$. The individual inductance upper bound is set to 4.2 mH (approximately $0.68\,L_{\max}$) to ensure that neither L_1 nor L_2 alone approaches the total inductance limit, reserving design margin for the other inductor. The lower bound of 0.2 mH is derived from equation (8) at rated current. Accordingly, the following search ranges are adopted for the optimization: $L_1 \in (0.2\,\text{mH}, 4.2\,\text{mH})$, $L_2 \in (0.2\,\text{mH}, 4.2\,\text{mH})$, and $C \in (2\,\mu\text{F}, 16\,\mu\text{F})$.

The optimized values of L_1, L_2, C and R_d can be obtained by employing the suggested MHTs as shown in Figure 7. Figure 7(a)–(d) show the optimization processes of L_1, L_2, C, and R_d,

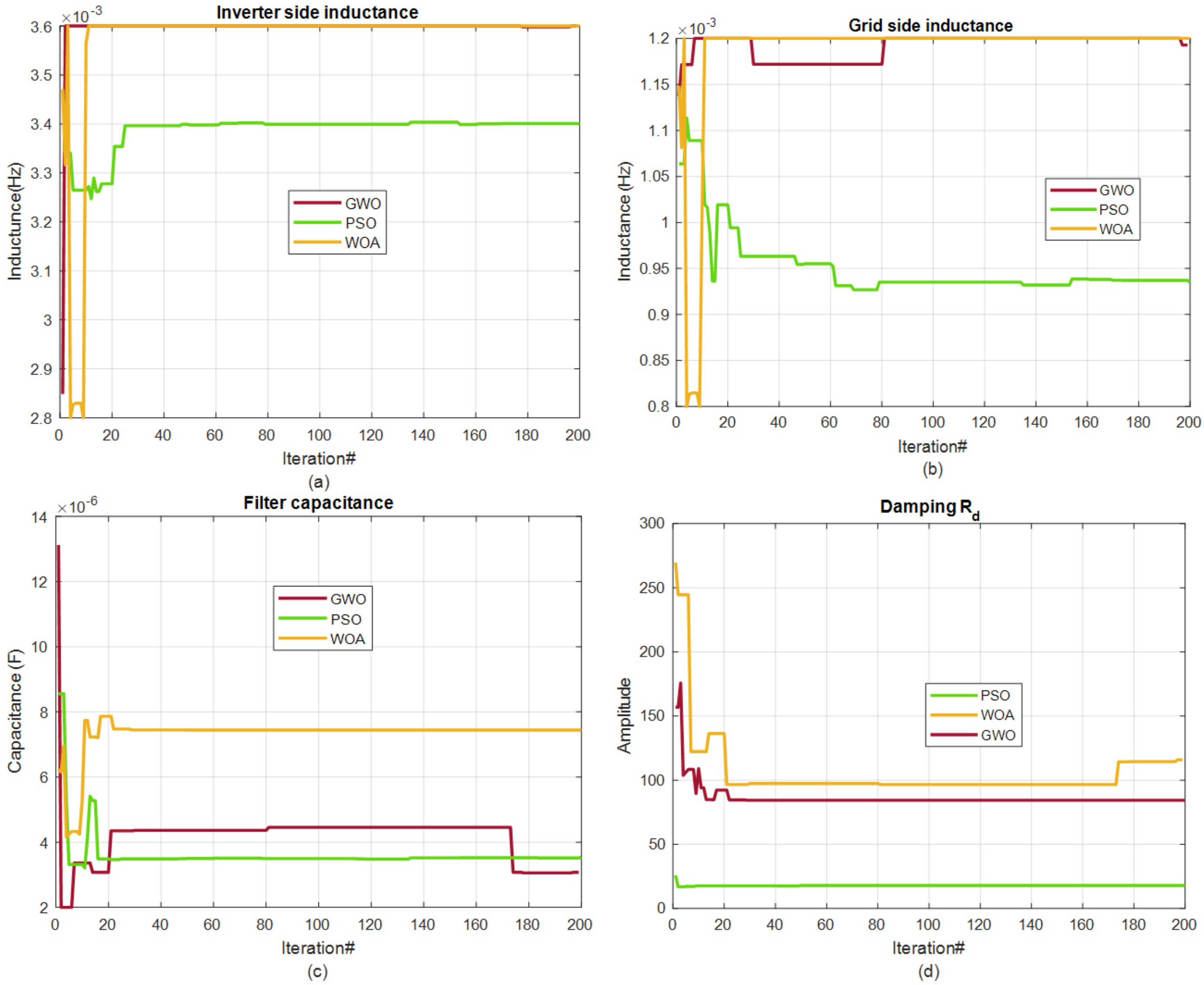

Figure 7. Optimization of LCL filter components using MHTs (a) L_1 (b) L_2 (c) C (d) R_d.

Table 2. GCI parameters.

Parameters	Symbol	Value
DC-voltage	U_{DC}	400 V
Grid-voltage	V_g	220 V
Grid-frequency	f_L	50 Hz
Rated-Power	P_N	5.0 kW
Switching-frequency	f_{sw}	10 kHz
Sampling-frequency	f_s	10 kHz

respectively. Each optimization method for LCL-filter parameters converges to a steady state after a specific number of iterations, signifying that the optimal solution has been reached. From Figure 7, it can be seen that PSO and GWO achieve a steady state faster than WOA. Moreover, with PSO, the values of L_1 and L_2 are less than the values achieved for the other two applied algorithms, which means the inductance value is also decreased. The optimization results achieved for the LCL components and damping resistor are given in Table 3.

Moreover, the power loss is shown in Figure 8(a), where it can be seen that the PSO technique results in lower losses than the other two MHTs. Figure 8(b) depicts how the fitness function changes over time. The figure makes it very evident that over the majority of the optimization process, the fitness value for each of the three MHTs that are selected is less than 1. It shows that the LCL components acquired during optimization are suitable for the initial optimization targets, and the related fitness value that is ultimately achieved is the lowest possible value. This implies that the THD has been reduced. However, the fitness value of the PSO algorithm is lower than that of the

Table 3. Optimized LCL filter components and damping coefficient using simulated MHTs.

Algorithm	L_1 (H)	L_2 (H)	C (F)	R_d (Ω)
WOA	3.6×10^{-3}	1.2×10^{-3}	7.4×10^{-6}	117
GWO	3.6×10^{-3}	1.18×10^{-3}	3.0×10^{-6}	87.9
PSO	3.43×10^{-3}	0.94×10^{-3}	3.5×10^{-6}	39.7

other algorithms; therefore, it shows the best results among the selected MHTs. These findings demonstrate the PSO supremacy in terms of its exploitation and exploration abilities for both local and global searches.

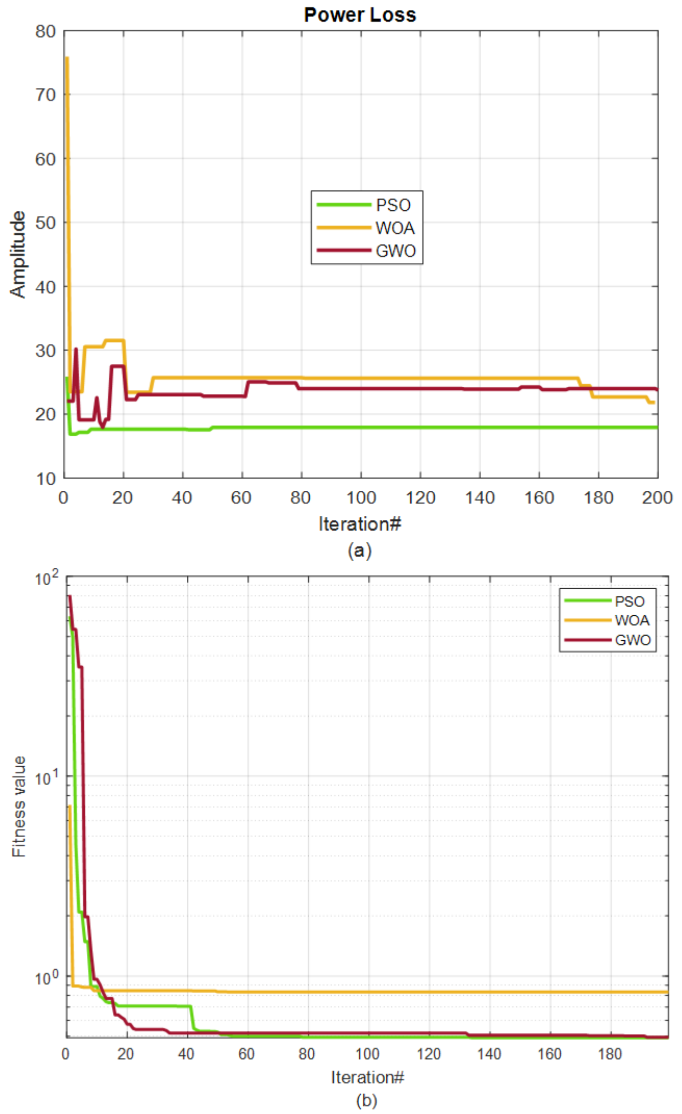

Figure 8. (a) Power loss (b) Objective function convergence with various MHTs.

6 System Simulation

To validate the effectiveness of the optimized design parameters, a comparative simulation study is designed using the preferred MHTs in the MATLAB/Simulink environment. The simulation model replicated the single-phase grid-tied VSI system with an LCL filter, as depicted in Figure 1 (a). The simulation utilized the parameters specified in Tables 2 and 3.

The transient and steady-state responses for current are simulated in Figure 9. The current control loop's performance is evaluated by introducing a 50% step change in the desired current. In Figure 9(a), the single-phase current tracks the desired current effectively for all the MHTs. Nevertheless, the overshoot is smaller in the case of the parameters obtained with the PSO algorithm compared with the other algorithms. The THD of current during the transition time increases to almost 2.8%, which is still acceptable because the IEEE standards (IEC 61,727 and IEEE 1547) allow a THD of 5% for GCIs. In the case of the PSO algorithm, the overshoot value of the system during the transient is between 4% and 5%, making it the MHT with the best performance among those that have been tested.

Moreover, Figure 9(b) illustrates the power of the system in response to a sudden change in the desired current. The active power increases with the increase in current and reaches a steady state within 0.02s. It is clear from Figure 9(b) that oscillations in active power arise without substantial overshoot value during the 50% step change in the desired current from its rated value. The oscillations in power during the steady state are acceptable. When the power achieves its steady state following a step change in the current desired, the findings reveal that the PSO optimization method gives less oscillations when compared with other MHTs.

To assess the system's robustness, a short circuit is introduced from 0.1s to 0.13s, as shown in Figure 10. A 0.25-ohm resistor is added in series with the grid to increase the challenge, forcing the current to flow through the short circuit wires. As seen in Figure 10(a), the grid RMS voltage drops by 90% during the short circuit. However, after the fault is cleared, the grid voltage recovers quickly to its nominal value for all proposed MHTs. Figure 10(b) shows the RMS current

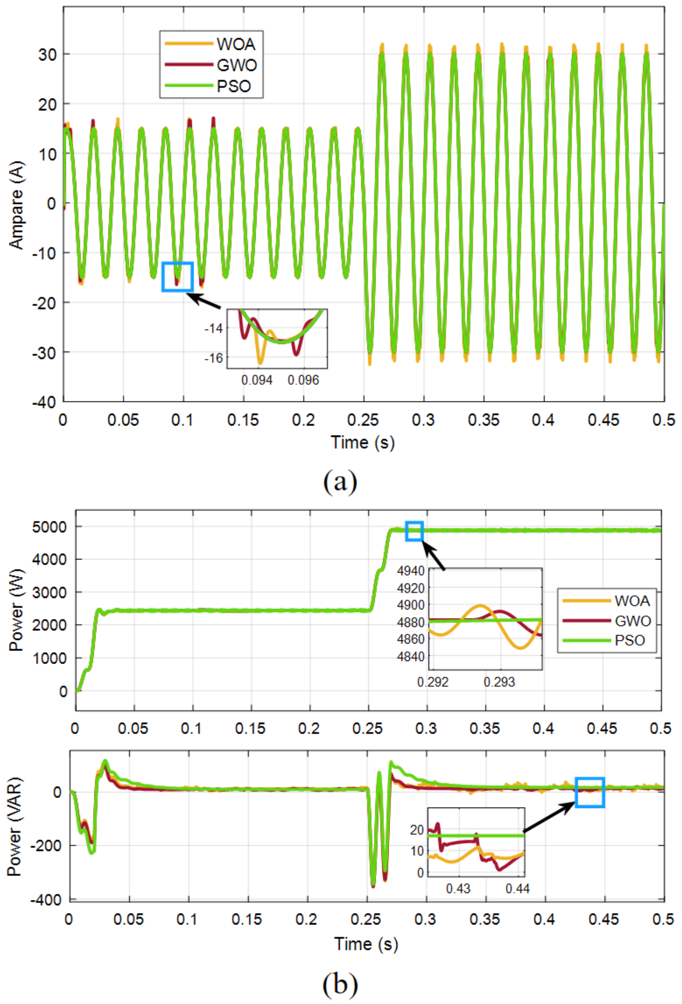

Figure 9. Response of simulated MHTs under varying desired current. (a) Current (b) Power.

during the short circuit fault. The figure indicates a smooth transition for all the selected MHTs; however, the oscillation in the case of the PSO algorithm is less than that of the other two algorithms. Moreover, the transient spike at the recovery time is also lower for the PSO algorithm. These simulation results show that the PSO-optimized components and damping resistance make it possible for the GCI system to be more stable and robust during a short-circuit failure.

Figure 10(c) shows the impact of the short circuit on the system's active and reactive power. During the short circuit, active power approaches zero, while reactive power displays transient behavior characterized by oscillations and transient spikes. These transient spikes are present for almost all three algorithms but are less prominent in PSO. These spikes can be removed by choosing a higher value for L1, which increases the cost of the filter. Therefore, these transients can be regarded as a trade-off between filter cost and performance. Following the short-circuit removal, both active and reactive power quickly return to their steady-state values. During the recovery process, the PSO algorithm shows lower oscillations

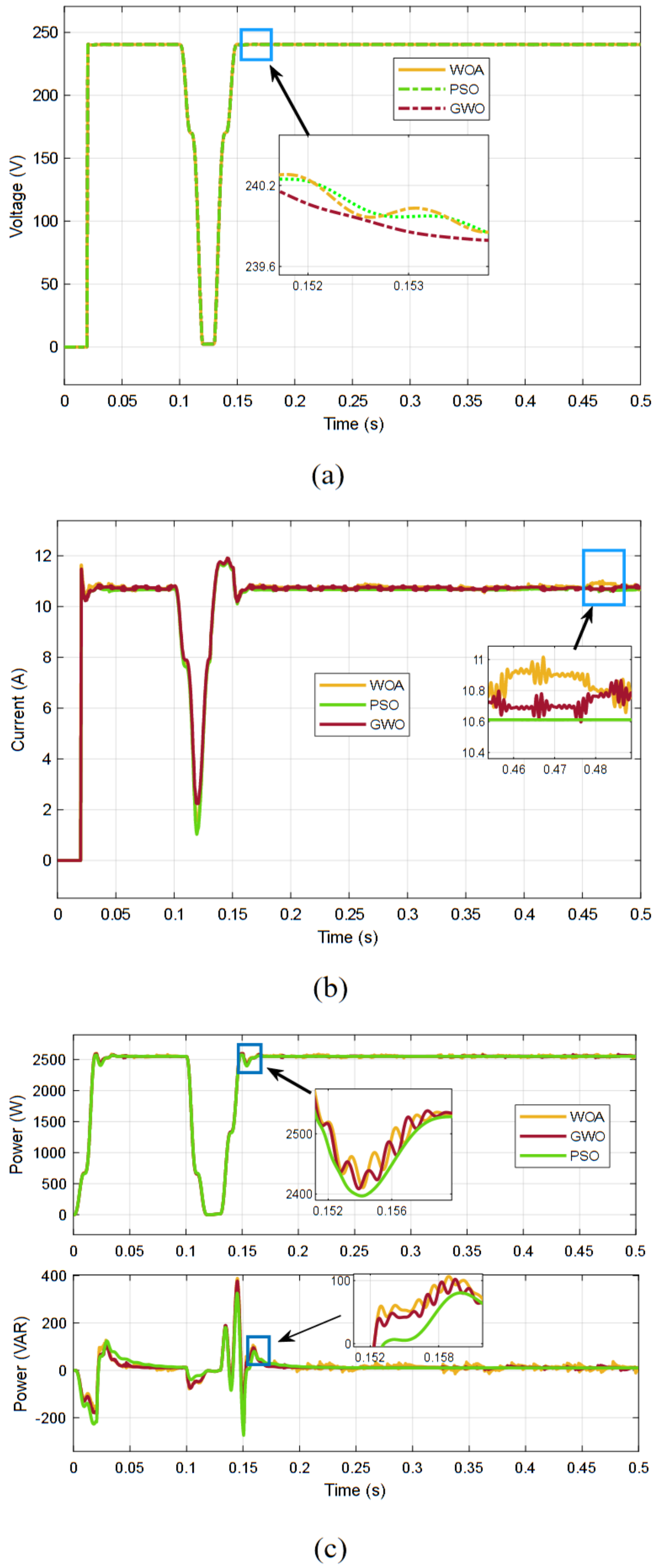

Figure 10. (a) Grid voltage (b) Injected current and (c) Power under short circuit.

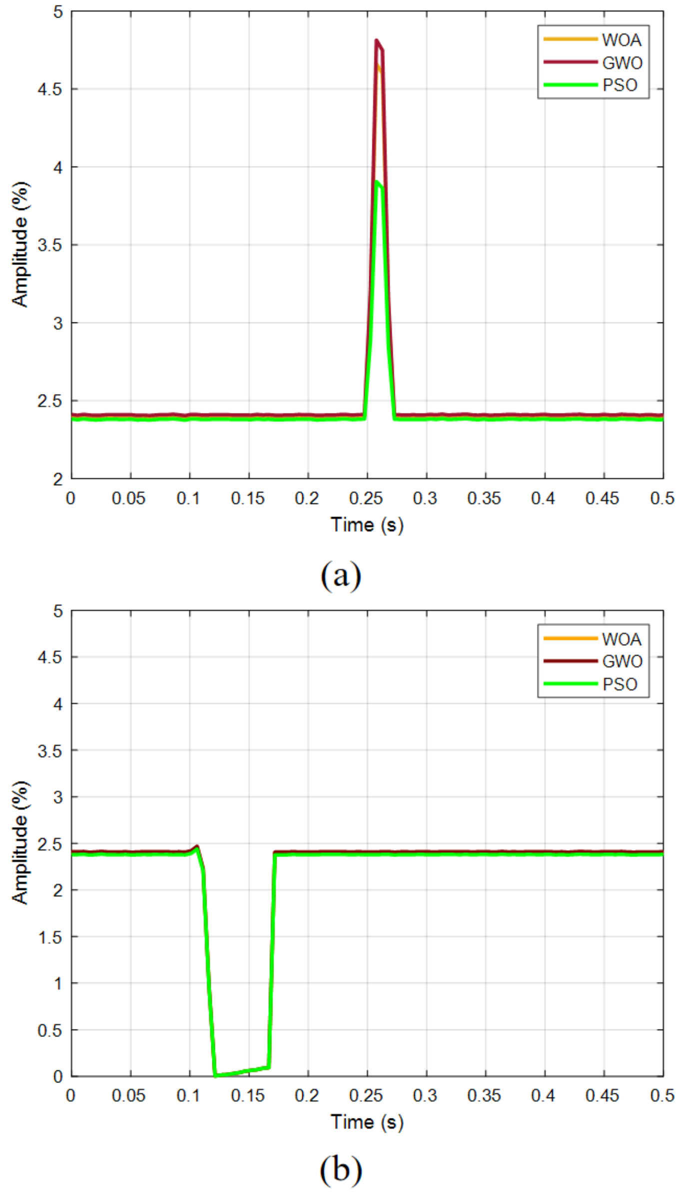

Figure 11. THD in injected current during (a) Step change in reference current (b) Grid short circuit test.

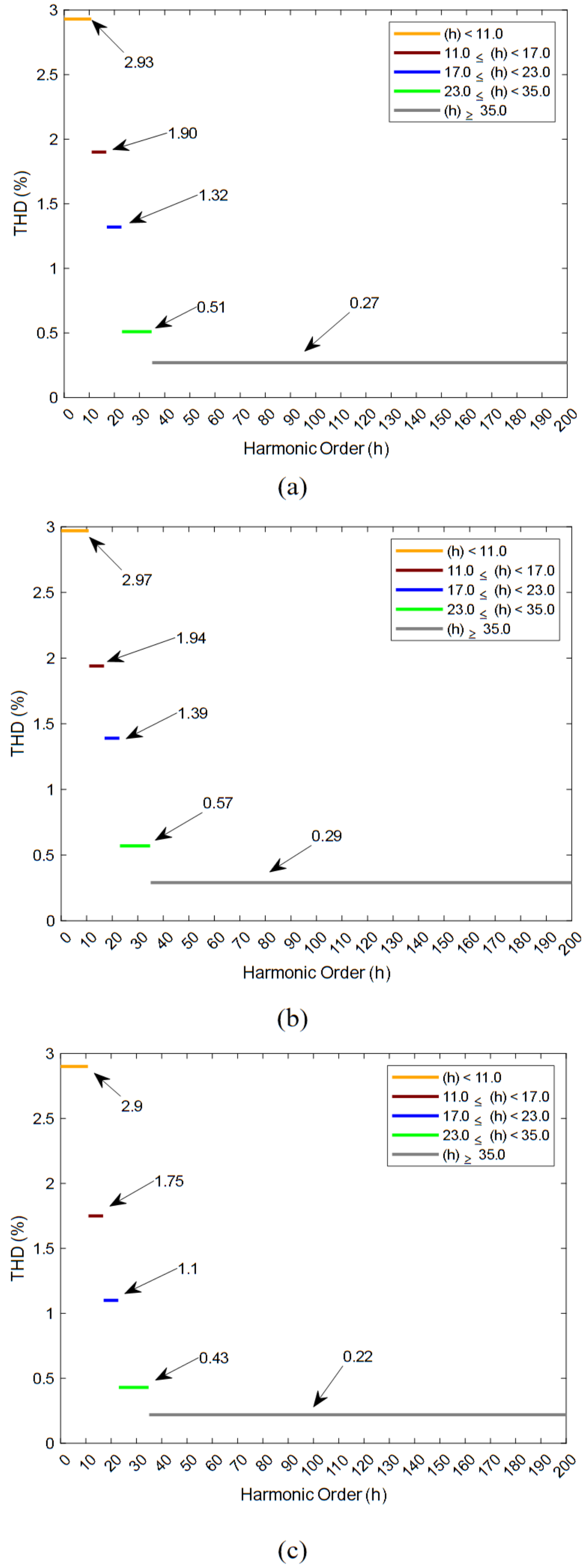

Figure 12. THD across harmonic orders for (a) WOA, (b) GWO and (c) PSO.

as compared with the other two algorithms. Based on these illustrative results, it is evident that in terms of robustness, stability, and dynamic response, the PSO algorithm surpasses the other two techniques for designing an LCL filter for GCI system.

Figure 11(a) illustrates the THD of the injected current during the step change in reference current. The THD of the grid-injected current remains within acceptable limits as per IEEE standards, even during the change in reference current. While it briefly exceeds 4% of the overall THD, it does not surpass the limit. Notably, during the transition, the THD for the PSO method remains lower than that of the other two applied algorithms. Similarly, Figure 11(b) presents the THD of grid-injected current during a grid short circuit test. It shows that, as the short circuit occurs, the THD exhibits a transient response in all cases before approaching 0.01% as the short circuit is removed, ultimately restoring to its original level. The PSO algorithm demonstrates the best response among the three simulated methods, indicating that the optimized LCL filter, damping resistor value and PR controller gains obtained through PSO are most effective for a single-phase GCI system.

Figure 12 illustrates the THD across various harmonic orders, as detailed in Table 1. The THD values remain within acceptable limits for all evaluated algorithms, demonstrating their effectiveness in managing harmonic content. Among these, PSO exhibits the best performance, achieving the lowest THD across the specified ranges as shown in Figure 12(c).

The WOA follows closely, showing the second-best performance with the least THD across each harmonic order in the injected current, as shown in Figure 12(a). Conversely, the GWO algorithm displays the highest THD distribution among the applied algorithms; however, it still remains within acceptable limits, as indicated in Figure 12(b). This analysis underscores the strengths of PSO and WOA in minimizing distortion while highlighting GWO's relative performance.

7 Conclusion

This paper presented a systematic computational study on the application of AI-driven metaheuristic optimization to the constrained parameter design of LCL filters in single-phase grid-connected inverter systems. A unified optimization framework was established, comprising a THD-minimization objective function and three engineering constraints, providing a well-defined benchmark for evaluating the computational performance of swarm-intelligence and evolutionary algorithms. Among the three algorithms evaluated—PSO, WOA, and GWO—PSO demonstrated the best overall computational behavior, achieving the lowest fitness value, fastest convergence, and highest solution quality in terms of filter parameter optimization. The PSO-optimized parameters yielded superior system robustness under both transient step-change conditions and weak-grid short-circuit faults, with THD maintained within IEEE 519 limits across all tested harmonic orders. These results establish PSO as the preferred computational method for this class of nonlinearly constrained engineering optimization problems. More broadly, the findings contribute to the growing body of evidence supporting the effectiveness of bio-inspired AI optimization algorithms in interdisciplinary computing applications, and provide a replicable methodological framework for future comparative studies involving alternative or hybrid metaheuristic strategies.

Data Availability Statement

Data will be made available on request.

Funding

This work was supported without any funding.

Conflicts of Interest

The authors declare no conflicts of interest.

AI Use Statement

The authors declare that no generative AI was used in the preparation of this manuscript.

Ethical Approval and Consent to Participate

Not applicable.

References

[1] Wu, T.-F., Misra, M., Jhang, Y.-Y., Huang, Y.-H., & Lin, L.-C. (2018). Direct digital control of single-phase grid-connected inverters with LCL filter based on inductance estimation model. *IEEE Transactions on Power Electronics*, *34*(2), 1851-1862. [CrossRef]

[2] Liserre, M., Blaabjerg, F., & Dell'Aquila, A. (2004). Step-by-step design procedure for a grid-connected three-phase PWM voltage source converter. *International journal of electronics*, *91*(8), 445-460. [CrossRef]

[3] Saïd-Romdhane, M. B., Naouar, M. W., Belkhodja, I. S., & Monmasson, E. (2016). Simple and systematic LCL filter design for three-phase grid-connected power converters. *Mathematics and Computers in Simulation*, *130*, 181-193. [CrossRef]

[4] Adamas-Pérez, H., Ponce-Silva, M., Mina-Antonio, J. D., Claudio-Sánchez, A., Rodríguez-Benítez, O., & Rodríguez-Benítez, O. M. (2024). A New LCL Filter Design Method for Single-Phase Photovoltaic Systems Connected to the Grid via Micro-Inverters. *Technologies*, *12*(6), 89. [CrossRef]

[5] Ali, R., Heydari-doostabad, H., Sajedi, S., & O'Donnell, T. (2024). Improved design of passive damping for single phase grid-connected LCL filtered inverter

considering impedance stability. *IET Power Electronics, 17*(4), 511-523. [CrossRef]

[6] Bierhoff, M., & Soliman, R. (2020). Analysis and design of grid-tied inverter with LCL filter. *IEEE Open Journal of Power Electronics, 1*, 161-169. [CrossRef]

[7] Beres, R. N., Wang, X., Blaabjerg, F., Liserre, M., & Bak, C. L. (2015). Optimal design of high-order passive-damped filters for grid-connected applications. *IEEE Transactions on Power Electronics, 31*(3), 2083-2098. [CrossRef]

[8] Wu, W., He, Y., Tang, T., & Blaabjerg, F. (2013). A new design method for the passive damped LCL and LLCL filter-based single-phase grid-tied inverter. *IEEE Transactions on Industrial Electronics, 60*(10), 4339-4350. [CrossRef]

[9] Wu, F., Sun, Z., Xu, W., Li, Z., & Lyu, J. (2022). A Control Parameters Design Method With Multi-Constrains for an LCL-Filtered Grid-Connected Inverter in a Weak Grid. *Frontiers in Energy Research, 9*, 798793. [CrossRef]

[10] Jalili, K., & Bernet, S. (2009). Design of $ LCL $ filters of active-front-end two-level voltage-source converters. *IEEE Transactions on Industrial Electronics, 56*(5), 1674-1689. [CrossRef]

[11] Khan, D., Qais, M., Sami, I., Hu, P., Zhu, K., & Abdelaziz, A. Y. (2023). Optimal LCL-filter design for a single-phase grid-connected inverter using metaheuristic algorithms. *Computers and Electrical Engineering, 110*, 108857. [CrossRef]

[12] Reznik, A., Simoes, M. G., Al-Durra, A., & Muyeen, S. M. (2013). $ LCL $ filter design and performance analysis for grid-interconnected systems. *IEEE transactions on industry applications, 50*(2), 1225-1232. [CrossRef]

[13] Jayalath, S., & Hanif, M. (2016). Generalized LCL-filter design algorithm for grid-connected voltage-source inverter. *IEEE Transactions on Industrial Electronics, 64*(3), 1905-1915. [CrossRef]

[14] Jayalath, S., & Hanif, M. (2017). An LCL-filter design with optimum total inductance and capacitance. *IEEE Transactions on Power Electronics, 33*(8), 6687-6698. [CrossRef]

[15] Wu, T. F., Misra, M., Lin, L. C., & Hsu, C. W. (2017). An improved resonant frequency based systematic LCL filter design method for grid-connected inverter. *IEEE Transactions on Industrial Electronics, 64*(8), 6412-6421. [CrossRef]

[16] Channegowda, P., & John, V. (2010). Filter optimization for grid interactive voltage source inverters. *IEEE Transactions on Industrial Electronics, 57*(12), 4106-4114. [CrossRef]

[17] Tong, L., Chen, C., & Zhang, J. (2019). Iterative design method of LCL filter for grid-connected converter to achieve optimal filter parameter combination. *The Journal of Engineering, 2019*(16), 1532-1538. [CrossRef]

[18] Meyer, R., & Mertens, A. (2012, September). Design and optimization of LCL filters for grid-connected converters. In *2012 15th International Power Electronics and Motion Control Conference* (*EPE/PEMC*) (pp. LS7a-1). IEEE. [CrossRef]

[19] Abbas, H. H., Shafiee, Q., & Bevrani, H. (2024). Optimal passive LCL filter design for grid-connected converters in weak grids. *Electric Power Systems Research, 235*, 110896. [CrossRef]

[20] Kim, Y. J., & Kim, H. (2019). Optimal design of LCL filter in grid-connected inverters. *IET Power Electronics, 12*(7), 1774-1782. [CrossRef]

[21] Wu, Z., Aldeen, M., & Saha, S. (2016, November). A novel optimisation method for the design of LCL filters for three-phase grid-tied inverters. In *2016 IEEE Innovative Smart Grid Technologies-Asia* (*ISGT-Asia*) (pp. 214-220). IEEE. [CrossRef]

[22] Hernandez, O., Mina, J., Calleja, J. H., Pérez, A. C., & de Leon, S. E. (2021). A multi-objective optimized design of LCL filters for grid-connected voltage source inverters considering discrete components. *International Transactions on Electrical Energy Systems, 31*(10), e12908. [CrossRef]

[23] Cai, Y., He, Y., Zhou, H., & Liu, J. (2021). Design method of LCL filter for grid-connected inverter based on particle swarm optimization and screening method. *IEEE Transactions on Power Electronics, 36*(9), 10097-10113. [CrossRef]

[24] Langella, R., Testa, A., & Alii, E. (2014). IEEE recommended practice and requirements for harmonic control in electric power systems. In *IEEE recommended practice*. IEEE. [CrossRef]

[25] Daley PE DGCP, I. L. S. M., & Houser PE, I. M. (2018). White Paper-Assessment of DER Interconnection Installation for Conformance with IEEE Std 1547. *Assessment of DER Interconnection Installation for Conformance with IEEE Std 1547*, 1-18. https://ieeexplore.ieee.org/servlet/opac?punumber=8305684

[26] Han, Y., Yang, M., Li, H., Yang, P., Xu, L., Coelho, E. A. A., & Guerrero, J. M. (2019). Modeling and stability analysis of $ LCL $-type grid-connected inverters: A comprehensive overview. *IEEE Access, 7*, 114975-115001. [CrossRef]

[27] Mirjalili, S., & Lewis, A. (2016). The whale optimization algorithm. *Advances in Engineering Software, 95*, 51-67. [CrossRef]

[28] Wang, D., Tan, D., & Liu, L. (2018). Particle swarm optimization algorithm: an overview. *Soft Computing, 22*(2), 387-408. [CrossRef]

[29] Mirjalili, S., Mirjalili, S. M., & Lewis, A. (2014). Grey wolf optimizer. *Advances in Engineering Software, 69*, 46-61. [CrossRef]

[30] Khan, D., Zhu, K., Hu, P., Waseem, M., Ahmed, E. M., & Lin, Z. (2023). Active damping of LCL-filtered grid-connected inverter based on parallel feedforward compensation strategy. *Ain Shams Engineering Journal,*

14(3), 101902. [CrossRef]

[31] Ruan, X., Wang, X., Pan, D., Yang, D., Li, W., & Bao, C. (2018). *Control techniques for LCL-type grid-connected inverters*. Springer Singapore. [CrossRef]

[32] Pena-Alzola, R., Liserre, M., Blaabjerg, F., Sebastián, R., Dannehl, J., & Fuchs, F. W. (2012). Analysis of the passive damping losses in LCL-filter-based grid converters. *IEEE transactions on power electronics*, *28*(6), 2642-2646. [CrossRef]

Imad Hussain completed his bachelor's degree at the COMSATS Institute of Information Technology, Islamabad, Pakistan in 2017 and received his master's degree from Shanghai Jiao Tong University, China in 2021. He is currently pursuing his doctoral degree at Wuhan University, China. His research interests span three key domains: (1) Advanced analysis and optimization of Series resonant Dual Active Bridge (SR-DAB) Converters for green hydrogen production. (2) Dual Active Bridge Converters for fuel cell applications, emphasizing soft-switching techniques, wide voltage range. (3) Power Converter Design & Renewable Energy Integration, Topology analysis and optimization of DC-DC and DC-AC converters for high-power applications. (Email: Imad_hussain@whu.edu.cn; imeekhan9@gmail.com)

Yigang He received his M.S. degree in electrical engineering from Hunan University, Chang sha, China; and his Ph.D. degree in electrical engineering from Xi'an Jiaotong University, Xi'an, China. He began his academic career at Hunan University, where he became a professor in 1999. Since 2017, he has been the vice-head of the School of Electrical Engineering, Wuhan University, Wuhan, China. His current research interests include power electronic circuits, smart grids, and fault diagnosis. He has over 300 publications in journals and conference proceedings. He has been a recipient of numerous awards, including being named among the world's top 2% scientists by Stanford University, Stanford, CA, USA. (Email: Yghe1221@whu.edu.cn)

Atta Ullah Khan received his B.Sc degree in electrical engineering from the Federal Urdu University of Arts, Science and Technology (FUUAST), Islamabad, Pakistan; and his M.S. degree in electrical engineering from COMSATS University, Islamabad, Pakistan. He is presently working towards his Ph.D. degree at Wuhan University, China. His current areas of interest in research include Renewable Energy Technologies, LED drivers, battery chargers, resonant converters, fixed frequency wide-range resonant converters, high-frequency soft-switching converters, and power electronics systems. (Email: attaktk333@gmail.com)

Yaqoob Ali was born in Khyber, Pakistan, in 1988. He received the B.Sc. and M.S. degrees in electrical engineering from the CECOS University of IT and Emerging Sciences, Peshawar, Pakistan, in 2011 and 2014, respectively. He is currently pursuing the Ph.D. degree in electrical engineering from Shanghai Jiao Tong University, Shanghai, China. From 2013 to 2015, he was a Research Assistant and a Lab Engineer with the CECOS University of IT and Emerging Sciences. Since 2016, he has been a Lecturer with the Electrical Engineering Department, University of Engineering and Technology at Peshawar, Peshawar. His current research interests include power converters and magnetic circuits. (Email: yaqoobali07@sjtu.edu.cn)

Idrees Khan received the BS degree in Electrical Engineering from Sarhad University of Engineering and Technology, Peshawar, Pakistan. Currently, he is a PhD student at the School of Automation and Electrical Engineering, Zhejiang University of Science and Technology, Shanghai, China. His research interests include robotics and control, automation, AI, machine learning, etc.. (Email: idreeskh5571@gmail.com)